

Article

Anionic Dye Alizarin Red S Removal Using Heat-Treated Dolomite

Zhaohui Li ^{1,*}, Anna Bowman ¹, Angie Rayniak ¹ and Shangping Xu ²

¹ Department of Geosciences, University of Wisconsin—Parkside, 900 Wood Road, Kenosha, WI 53144, USA; fiebe001@rangers.uwp.edu (A.R.)

² Department of Geosciences, University of Wisconsin Milwaukee, 3209 N. Maryland Ave., Milwaukee, WI 53211, USA

* Correspondence: li@uwp.edu

Abstract: In modern society, frequent use of synthetic materials in the household and industry presents a great challenge to environmental and water quality. As such, numerous types of research have been conducted for potential removal of emerging contaminants from water using advanced materials. Earth materials, due to their low costs and vast reserves, have also been evaluated in great details for contaminant removal. In this study, a naturally occurring carbonate mineral dolomite (Dol) was assessed for the removal of an anionic dye alizarin red S (ARS) from aqueous solution before and after heat treatment to increase its performance. The ARS-removal capacities increased from 80 to 130 mmol/kg after heat treatment based on the isotherm study. And the ARS-removal efficiency rose by a factor of four as the partitioning coefficient increased from 1.5 to 6 L/mmol after heat treatment. The X-ray diffraction (XRD) analyses showed minute conversion of dolomite into calcite after samples being heated at 800 °C for 3 h. However, there were no phase changes for ARS before and after its sorption. Fourier transform infra-red (FTIR) results also showed a minute appearance of calcite after heating. Thus, the increase in ARS sorption could be due to surface reactivation of Dol after heating or due to formation of a minute amount of amorphous MgO in the system as a result of the conversion of Dol to calcite. The results from this study will add new perspectives to the utilization of Earth materials for environmental application.

Keywords: color dyes; complexation; dolomite; heat treatment; removal; sorption



Citation: Li, Z.; Bowman, A.; Rayniak, A.; Xu, S. Anionic Dye Alizarin Red S Removal Using Heat-Treated Dolomite. *Crystals* **2024**, *14*, 187. <https://doi.org/10.3390/cryst14020187>

Academic Editor: Maria Milanova

Received: 22 January 2024

Revised: 8 February 2024

Accepted: 11 February 2024

Published: 13 February 2024



Copyright: © 2024 by the authors. Licensee MDPI, Basel, Switzerland. This article is an open access article distributed under the terms and conditions of the Creative Commons Attribution (CC BY) license (<https://creativecommons.org/licenses/by/4.0/>).

1. Introduction

The use of color dyes over the last half-century increased drastically [1]. In a review article published in 2009, it was stated that about 100,000 types of dyes with a mass of 7×10^5 to 1×10^6 tons were manufactured each year [2]. In the textile industry, once the dyeing process was finished, the waste, which could contain as much as 85% of the initial dye, was often discharged into the environment [3], which could significantly impair the quality of the receiving aquatic system [4]. For example, when the amount of residual dye in wastewater increased, color, pH, chemical, and biological oxygen demands as well as metal concentration of wastewater will change correspondingly [5]. As such, extensive studies for dye removal from water were conducted in the last several decades and various physical, chemical, and biological removal methods have been explored [3]. Adsorption represents an excellent physical method for the removal of a wide variety of dyes but one typical disadvantage of the adsorption method is high material cost associated with many industrial adsorbents [3]. Thus, many attempts were made to focus on searching for sorbents with high efficacy and low material costs and many Earth materials, particularly clay minerals, fall into this category [6–9].

In addition to clay minerals, carbonate minerals such as calcite (Cal) and dolomite (Dol) were also studied for the removal of color dyes before and after heat treatment. Previous results showed that Dol will decompose into Cal, magnesium oxide, and carbon

dioxide at temperatures of 700 °C [10,11], 800 °C [12,13], or 900 °C [14]. Dol heated at 800 °C for 4 h was evaluated for the removal of dyes basic violet 16 (BV₁₆, C₂₃H₂₉ClN₂) and reactive red 195 (RR195, C₃₁H₁₉ClN₇Na₅O₁₉S₆) from initial concentrations of 10 to 50 mg/L (constant mass volume ratio of 1.5 g/0.5 L of solution) [15]. Also, Dol heated for 5 h at 300, 700, and 900 °C was evaluated for the removal of methyl orange (MO), C.I.13025, (C₁₄H₁₄N₃NaO₃S) [14]. In a binary solution made of reactive black 5 (RB5) and Congo red (CR), Dol treated at 900 °C showed preferential adsorption of CR over RB5 and was attributed to inner-sphere complexation with amine groups since CR and RB5 contain two vs. one amine functional groups [16]. In addition, Dol-modified biochar was evaluated for the efficient removal of anionic dyes remazol brilliant blue (RBB) and RB5 from simulated wastewater solutions in a recent study with a sorption capacity of 33 and 23 mg/g for RBB and RB5, respectively [17]. However, neither the Dol nor the pristine rice husk biochar were tested for comparison. And the mechanism of Dol modification was not discussed, either. Studies on methylene blue (MB) removal by alkaline-activated Dol showed a capacity of 350 mg/g but no evaluation of original Dol was provided for comparison [18].

Alizarin red S (ARS) is an anionic dye made of typical dihydroxyanthraquinone and was derived from the roots of plants of the madder genus and was originally used as a traditional dye [19]. It has also been used over decades for the evaluation of calcium-rich deposits in cells. It is particularly versatile, as the dye can be extracted from the stained monolayer and assayed [20]. It can also react with Mg and other group II elements and form complexes with other divalent transition metals [19]. As most Earth materials have negative charges on their surfaces, organic materials such as synthetic carbon nanotubes were evaluated for ARS removal [21]. For inorganic materials, layered double hydroxide (LDH) was evaluated for ARS removal due to its positively charged surfaces [22]. Removal of ARS from aqueous media using alumina as an adsorbent was also studied under different physico-chemical conditions but the removal capacity was not mentioned [23].

ARS was initially used for the identification of carbonate minerals [24]. The stain was more for aragonite, Cal, witherite, and cerussite, as these minerals dissolve more rapidly in dilute HCl in comparison to Dol, siderite, magnesite, and rhodochrosite, which react much slower with the acid and remained unstained [25]. Later, it was found that it was sorbed more on apatite than on Cal and the sorption was controlled more by its -OH groups rather than the -SO₃ group [26].

Due to the strong affinity of ARS for calcium and phosphorus, calcium phosphate hydroxyapatite (Ca-Hap) was synthesized from CaCO₃ and H₃PO₅ and its removal of ARS was assessed under different physico-chemical conditions with an ARS removal capacity of 100 mg/g [27]. Also, the complexation of ARS with Ca²⁺ on surface of fluorite (CaF₂) was studied in detail [28].

A literature survey about eight years ago showed that dye sorption by Dol was almost non-existent [16]. Removal of RB5, an anionic dye, by Dol after heat treatment resulted in a capacity of 126 mg/g [16]. Similarly, Dol after being heated to 800 °C also showed a sorption capacity of 73 mg/g for RR195, another anionic dye [15,29]. Calcinated Dol at 1100 °C, at which the Dol decayed to CaO, MgO, Ca(OH)₂, and Mg(OH)₂, was also evaluated for the removal of humic acid with a capacity about 22 to 35 mg/g [30].

Although several studies have reported the removal of color dyes using heat-treated Dol, no report could be found for the removal of anionic dye ARS by Dol before or after heat treatment. To fill this knowledge gap, in this study, we quantified and compared the removal of ARS by Dol before and after heat treatment under different physico-chemical conditions. The sorbents were characterized after ARS sorption. The mechanisms of interactions between ARS and the sorbents were speculated. Overall, the results of this study would provide new perspectives for the utilization of Earth materials for environmental remediation and water treatment. Specifically, the bedrocks in southeastern Wisconsin, where the universities of the authors are located, are Devonian dolomite. Thus, the findings from this study could promote local and regional business initiatives to actively find new use of local resources for global environmental application.

2. Materials and Methods

2.1. Materials

The dolomite (Dol), whose composition is $\text{CaMg}(\text{CO}_3)_2$, was from the stock dolomite mineral in the Geosciences Department, University of Wisconsin – Parkside. The chemical composition of the Dol was characterized with X-ray diffraction (XRD). It was crushed with a mill crusher and then ground to less than 230 meshes (0.063 mm), in the silt size range. For heat treatment, 4 ceramic crucibles each with a mass of 8.0 g of ground Dol were placed inside a muffle furnace. Then, samples were heated to 600, 800, and 1000 °C, respectively, and maintained for 2–4 h with a heating rate about 30–40 °C/min. After heating, the samples were left inside the furnace overnight to cool to room temperature (23 °C). They were designated as HDol.

The size distributions of Dol and HDol were measured using the Malvern Mastersizer 2000 laser diffraction particle size analyzer. Briefly, the samples (~0.1 g) were suspended in 50 mL deionized water and laser beams were used to measure particle sizes in the range of 0.02 to 2000 μm . The Mie diffraction theory was then applied by the Mastersizer 2000 software to calculate particle sizes [31].

The anionic dye alizarin red S (ARS) is also referred to as nordant red 3 or alizarin carmine. Its IUPAC name is sodium; 3,4-dihydroxy-9,10-dioxo-9,10-dihydroanthracene-2-sulfonate. It has a formula of $\text{C}_{14}\text{H}_7\text{NaO}_7\text{S}$, a molecular mass of 342.253 g/mol, and CAS# of 130-22-3. It has Na^+ as its counterion. Its color changes from yellow at pH 3.5 to pink at pH 6.5, to orange–brown at pH 9.4, and, then, to violet at pH 12.0 (Acros). (<https://www.fishersci.com/shop/products/alizarin-red-s-pure-certified-acros-organics-2/AC400480250/#?keyword=alizarin%20s>, accessed on 12 February 2024). It has pK_a values of 5.49 and 10.85 [19], or 4.5 and 11 from Chemical Book (https://www.chemicalbook.com/ProductChemicalPropertiesCB0711917_EN.htm, accessed on 12 February 2024). Its dimension and the diagram of speciation against equilibrium solution pH is illustrated in Figure 1. It is water soluble with values varying from 1 g/L (https://www.chemicalbook.com/ChemicalProductProperty_EN_CB0711917.htm; <https://www.scbt.com/p/alizarin-red-s-130-22-3> accessed on 12 February 2024) to 7.69% (<https://us.vwr.com/store/product/17336548/alizarin-red-s-sodium-salt-certified-c-i-58005> accessed on 12 February 2024). Its melting point is 287–298 °C (<https://www.scbt.com/p/alizarin-red-s-130-22-3> accessed on 12 February 2024).

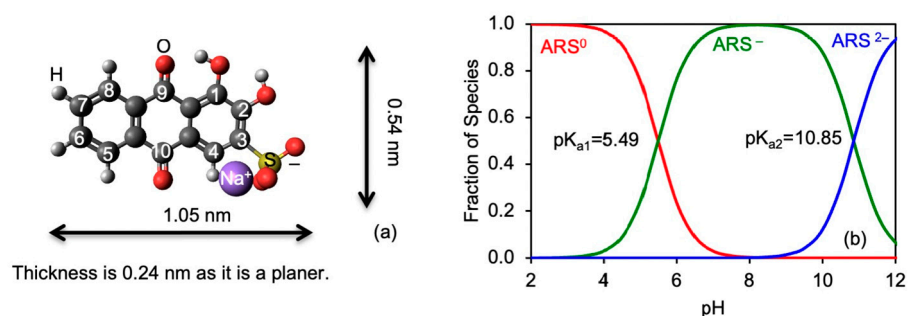


Figure 1. Molecular structures of ARS (a) and its pH-speciation diagrams (b).

2.2. Batch Studies

ARS concentrations of 0.1 and 0.2 mM were used for the initial evaluation of its adsorption by the HDol treated at 600, 800, and 1000 °C. Briefly, 0.5 g of solid and 10 mL of ARS solution were mixed in each 50 mL centrifuge tube at 150 rpm for 24 h. Then, the samples were centrifuged for 10 min at 3500 rpm. The supernatants were filtered by 0.45 μm syringe filters. The equilibrium ARS concentrations were determined using a UV-Vis spectrophotometer at the wavelength 420 nm. As the speciation of ARS is a function of aqueous pH (Figure 1b), calibration curves were prepared for different pH values and the concentrations of ARS were determined using the calibration curves of the specific pH

conditions. The results showed that the ARS removal was about 70% for Dol and HDol heated to 600 °C, and 99% for the HDol heated to 800 and 1000 °C. As such, the raw Dol and HDol heated to 800 °C, which exhibited optimal ARS removal capacity, were selected for further studies of ARS removal under different physico-chemical conditions (see below).

For all following adsorption experiments, the quantities of solid and liquid used were 0.5 g and 10 mL, respectively. To determine the sorption capacity, the initial ARS concentrations were 0.0, 0.2, 0.4, 1.0, 2.0, 3.0, 4.0, and 5.0 mM. The mixtures were shaken for 24 h at 150 rpm. Then, the samples were centrifuged for 10 min at 3500 rpm. The supernatants were filtered by syringe filters of 0.45 µm in pore size. The equilibrium ARS concentrations were determined using the UV-Vis method. Proper dilution was made when the absorbance values were greater than 1.000. For all other batch studies, the initial concentrations of ARS were 1.0 and 3.0 mM for Dol and HDol, respectively. To quantify ARS adsorption kinetics, the solid-liquid mixtures were shaken for varying amounts of time, ranging from ¼ to 24 h. To investigate the effects of ionic strength on ARS adsorption, the ionic strength was adjusted to 0.001, 0.01, 0.1, and 1.0 M NaCl. To evaluate how pH would affect ARS adsorption, proper amounts of concentrated HCl or NaOH were added to adjust the final equilibrium pH to about 3–11. Finally, the mixtures were shaken at 23, 33, 43, and 53 °C to study the temperature effect. The separation of supernatants from the solids was the same as mentioned before. The amount of dye sorbed was calculated by:

$$C_s \text{ (mmol/kg)} = (C_{\text{initial}} - C_{\text{Equilibrium}}) \frac{\text{Volume of liquids (mL)}}{\text{Mass of solid (g)}} \quad (1)$$

2.3. Methods of Analyses

After dye sorption, the solid samples were dried naturally and, then, analyzed by XRD and Fourier transform infrared (FTIR) to evaluate whether changes in structure or bonding happened after dye sorption. A Shimadzu 6100 X-ray diffractometer (Kyoto, Japan) with a Ni filter and a CuK α radiation at 30 kV and 40 mA was used for the XRD analyses. Samples were scanned at a speed of 2°/min from 20–60° (2 θ). A Shimadzu 8100 spectrometer (Kyoto, Japan) with a quartz ATR was used for FTIR analyses. Samples were scanned from 400 to 4000 cm⁻¹ with a resolution of 2 cm⁻¹.

The Dol and HDol samples before and after the dye adsorption experiments were also examined using a scanning electron microscope (SEM, model: Hitachi S-4800, Kyoto, Japan). For this purpose, the samples were mounted onto individual 13 mm aluminum stubs with carbon tape. The mounted samples were then coated with carbon in a vacuum coater (Edwards 306A coating system, Irvine, CA, USA). Images were captured using 10.0 kV accelerating voltage in high-current mode at 15.0 mm working distance. The elemental makeup of the samples was characterized through energy dispersive X-ray spectroscopy (EDS) using a Bruker Quantax Esprit system (Billerica, MA, USA).

3. Results

3.1. ARS Sorption Isotherm

Sorption of ARS on Dol and HDol is illustrated in Figure 2. Several isotherm models were used to fit the experimental data. The fitted parameters can be seen in Table 1. The Langmuir isotherm has the formula of:

$$C_s = \frac{K_L S_m C_L}{1 + K_L C_L} \quad (2)$$

where C_L and C_s represent ARS concentration in water (mmol/L) and amount of ARS sorbed on solid (mmol/kg), respectively. The solute sorption capacity is represented by

the Langmuir parameter S_m (mmol/kg) and affinity of the solute for the solid surface is represented by K_L (L/mmol). Equation (2) can be converted into a linear form:

$$\frac{C_L}{C_s} = \frac{1}{K_L S_m} + \frac{C_L}{S_m} \quad (3)$$

and the S_m and K_L can be calculated via a linear regression.

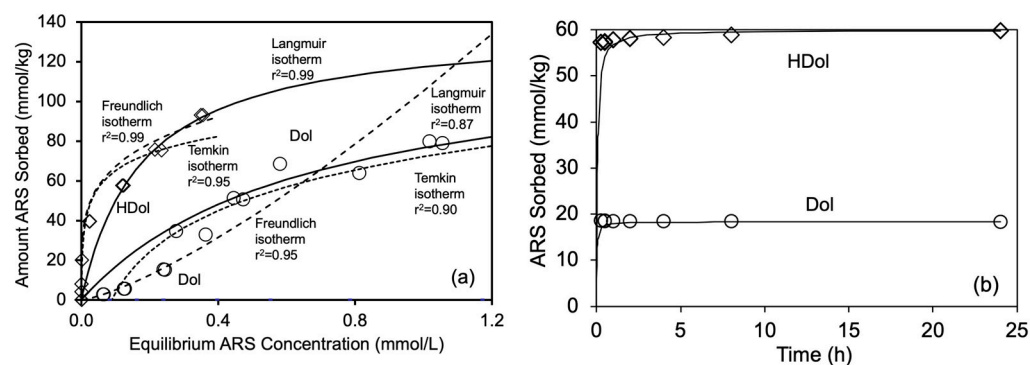


Figure 2. Sorption isotherms (a) and kinetics (b) of ARS on raw Dol (○) and HDol at 800°C (◇). The Langmuir, Freundlich, and Temkin fittings are indicated by solid, dashed, and dotted lines.

Table 1. Comparison of ARS sorption parameters using Dol and HDol as the sorbents.

Sorption Parameters	ARS Sorption on Dol	ARS Sorption on HDol
S_m (mmol/kg)	80	140
K_L (L/mmol)	1.5	6.0
r^2 for Langmuir isotherm fitting	0.71	0.96
K_F (L/kg)	105	113
$1/n$	1.3	0.2
r^2 for Freundlich isotherm fitting	0.95	0.99
q_e (mmol/kg)	18	60
kq_e^2 (mmol/kg-h)	833	1250
k (kg/mmol-h)	2.5	0.3
r^2 for pseudo-second-order fitting	0.9999	0.9999

Previous results showed that Langmuir sorption isotherm fitted the sorption of ARS and brilliant blue FCF on *Abelmoschus esculentus* stem powder well [32]. And ARS sorption capacity on synthetic LDH was 29 mg/g [22]. In this study, the ARS sorption capacity was about 80 mmol/kg on Dol based on the Langmuir isotherm fitting (Figure 2a). In comparison, the ARS sorption capacity on HDol is 138 mmol/kg, about 70% higher (Figure 2a). Meanwhile, the K_L value was about 6 L/mmol for HDol and 1.5 L/mmol for Dol, an increase in ARS affinity by a factor of 4 for HDol (Figure 2a). It was previously reported that the sorption of azo dye orange I by HDol heated to 900 °C also increased by a factor of 4 when compared to its adsorption by raw Dol [10].

In addition to the Langmuir model, data were also fitted to the Freundlich isotherm model. It has the formula of:

$$C_s = K_F C_L^{1/n} \quad (4)$$

in which the Freundlich isotherm constant is K_F and the intensity of the adsorption is $1/n$. When $1/n$ is $0 < 1/n < 1$, the sorption is favorable, while when $1/n$ is greater than 1, the sorption process is unfavorable [33]. The $K_F = 105$ and 113 while the $1/n = 1.3$ and 0.2 for ARS sorption on Dol and HDol, suggesting a favorable ARS sorption on HDol.

3.2. ARS Sorption Kinetics

Several kinetic models were used to fit the experimental data and the pseudo-second-order kinetic model had the best fit (Figure 2b). It has the formula of

$$q_t = \frac{kq_e^2 t}{1 + kq_e t} \quad (5)$$

And it can be converted into a linear form:

$$\frac{t}{q_t} = \frac{1}{kq_e^2} + \frac{1}{q_e} t \quad (6)$$

In above equations, the rate constant and initial rate of ARS sorption on solid surfaces are represented by k (kg/mmol/h) and kq_e^2 (mmol/kg/h). And q_t and q_e (mmol/kg) represent the amounts of ARS sorbed at time t and at equilibrium. For ARS sorption on Dol from an initial ARS concentration of 1.0 mM, the k was 2.5 kg/mmol/h and the q_e was 18.3 mmol/kg. In contrast, the k was 0.3 kg/mmol/h but the q_e was 60 mmol/kg for ARS sorption on HDol from an initial concentration of 3.0 mM. Moreover, the initial rates kq_e^2 were 833 and 1250 mmol/kg/h for ARS sorption on Dol and HDol, respectively (Table 1). Similarly, the pseudo-second-order kinetics model fitted the ARS sorption on synthetic LDH well with a k value of 0.008 L/mg/min [22]. Also, ARS sorption on halloysite from single and binary solution mixed with MB resulted in q_e values of 33.3 and 73 mmol/kg and kq_e^2 values of 222 and 256 mmol/kg/h [34]. For comparison, removal of RBB and RB5, both being anionic dyes, from simulated wastewater solutions using Dol-modified biochar also followed the pseudo-second-order kinetics well [17].

3.3. Effects of Equilibrium Solution pH, Ionic Strength, and Temperature on ARS Sorption

Previous studies showed that the adsorption of dyes by various adsorbents can be strongly influenced by water pH. For instance, the adsorption of alizarin (AZ) by calcium deposits peaked around pH 12 [35]. Removal of RBB and RB5 from simulated wastewater solutions using Dol-modified biochar, however, decreased significantly with an increase in solution pH [17]. For the dye of Janus green B, its adsorption by Algerian diatomite was not influenced by water pH [12]. In contrast, at initial concentrations of 25, 50, and 100 mg/L ARS sorption on mustard husk was 100% at pH 2 and it decreased to 45–50% at pH 9–10 [36]. In this study, ARS sorption on Dol was about 18 mmol/kg from pH 5 to 7. But the sorption decreased slightly to 13 mmol/kg at pH 12. Similarly, the adsorption of ARS by HDol was 55 to 57 mmol/kg for pH 5 to 9 and decreased slightly to 41 mmol/kg at pH 12 (Figure 3a). Our results showed that HDol could be an effective ARS remover when pH is lower than 11.

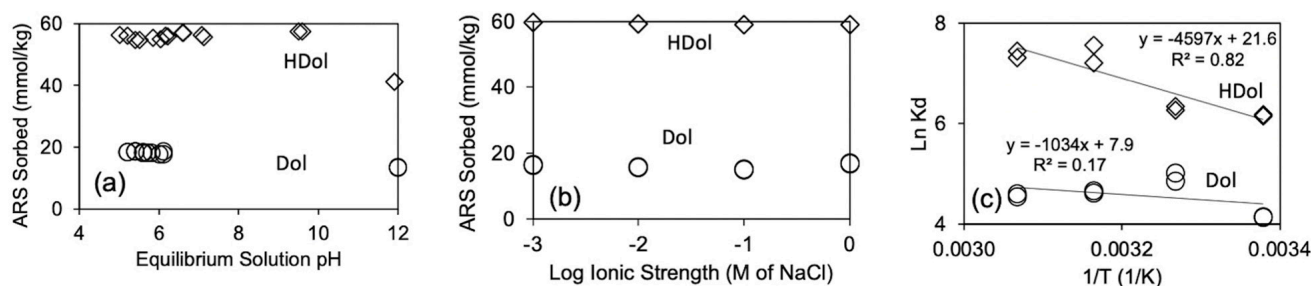


Figure 3. Influence of equilibrium solution pH (a), ionic strength (b), and temperature (c) on ARS sorption on Dol (○) and HDol (◇).

The influence of solution ionic strength on ARS sorption on Dol and HDol was minimal. For Dol, the ARS sorption was in the range of 15 to 17 mmol/kg. For HDol, the

ARS sorption was between 59 and 60 mmol/kg (Figure 3b), suggesting that the presence of anion chloride had minimal competition against anionic dye ARS sorption on Dol or HDol.

The influence of temperature on ARS sorption is demonstrated in Figure 3c. The thermodynamics for solute sorption from solution is governed by

$$\ln K_d = -\frac{\Delta H}{RT} + \frac{\Delta S}{R} \quad (7)$$

In the above equation, the solute distribution coefficient is represented by K_d , the changes in enthalpy and entropy after solute sorption are represented by ΔH and ΔS , and the gas constant and temperature in K are represented by R and T . The change in free energy ΔG after solute sorption related to ΔH and ΔS is governed by

$$\Delta G = \Delta H - T\Delta S \quad (8)$$

For ARS sorption on Dol and HDol, the ΔH values are 9 and 38 kJ/mol, the ΔS values are 0.07 and 0.18 kJ/mol/K and the ΔG values are -11 to -13 and -15 to -20 kJ/mol, respectively, suggesting that the sorption is spontaneous, endothermic, and resulting in increase in disorder of the sorbed dye molecules, and weak electrostatic interactions were responsible for the uptake of dye molecule on the mineral surfaces.

3.4. XRD Analyses

In a previous study, using the XRD indexing of ARS calculated before [37], the XRD peaks of crystalline ARS at 26.38, 31.72, and 45.44° (2θ) were attributed to the reflections of (−304), (222), and (−434). In this study, the XRD patterns of Dol and HDol before and after ARS sorption were presented in Figure 4. No change in the d -spacing of Dol nor diffraction peaks of ARS were found in these patterns, suggesting the sorption of ARS was on the external surfaces and no crystalline ARS was found on Dol or HDol surfaces. In comparison to the XRD patterns of Dol, those of HDol showed a peak at 29.38 to 29.42° (2θ), corresponding to the d_{104} diffraction peak of calcite with a spacing of 3.033 to 3.038 Å (Figure 4a), suggesting that only a minute amount of Dol was converted to calcite after being heated at 800°C for 3 h.

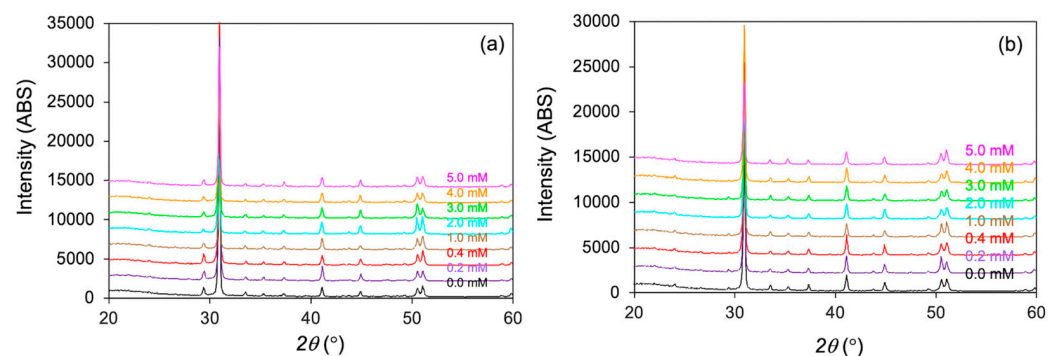


Figure 4. XRD patterns of HDol (a) and Dol (b) after ARS sorption from different initial concentrations.

The strongest peak of MgO is at 42.98° (2θ) [38] and this peak is not found on the XRD patterns of HDol, suggesting that no crystalline MgO was produced. Meanwhile, CaO had its characteristic (111) peak at 32.34° (2θ) and Ca(OH)_2 had its characteristic (101) peak at 34.11° (2θ) [39]. These peaks are not present in the XRD patterns of HDol either, suggesting neither was produced, or not in crystalline form, due to a minute conversion of dolomite to calcite after being heated at 800 °C for 3 h.

3.5. FTIR Analyses

For the FTIR of Dol, the ν_2 (CO_3^{2-}) band is at 881 cm^{-1} while the same band for calcite is at 875 cm^{-1} and the ν_3 (CO_3^{2-}) and in-plane bending ν_4 (CO_3^{2-}) bands for Dol are at

1400–1480 cm^{-1} and 713 cm^{-1} [40]. In this study, these bands are located at 876, 1414–1418, and 727 cm^{-1} for both Dol and HDol, again confirming that the raw Dol is pure and there was not much change after Dol was heated at 800°C for 3 h (Figure 5). In another study, the ν_4 (CO_3^{2-}) band was located at 713 cm^{-1} for calcite and 730 cm^{-1} for Dol [41]. The band at 730 cm^{-1} is especially useful for indicating the presence of Dol [42]. In this study it is located at 727 cm^{-1} for Dol, again confirming it is dolomite instead of calcite. For HDol, a minute shoulder at 713 cm^{-1} can be noticed, suggesting a minute amount of calcite is formed after heating, confirming the XRD results.

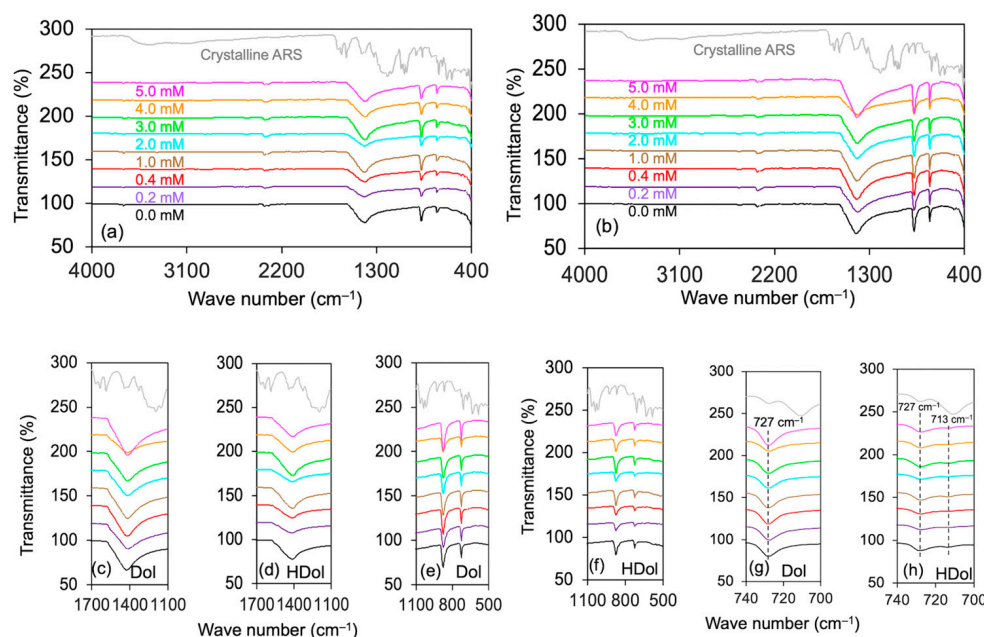


Figure 5. FTIR spectra of Dol (a) and HDol (b) after ARS sorption from different initial concentrations. And their enlargement at 1100 to 1700 cm^{-1} , 500 to 1100 cm^{-1} , and 700 to 740 cm^{-1} (c–h).

The characteristic bands of solid ARS were located at: 3448, 1643, 1589, 1546, 1191, 1069, 1037, and 1127 cm^{-1} for $\nu(\text{OH})$ of hydrogen bonding, $\nu(10\text{-C=O})$, $\nu(9\text{-C=O})$, $\nu(\text{Ar C=C})$, $\nu(\text{C-O})$, $\nu_{\text{as}}(\text{SO}_3)$, $\nu_{\text{s}}(\text{SO}_3)$, and carbonyl C–C–C [43]. However, none of these bands were observed on the samples of Dol or HDol after ARS sorption (Figure 5). At the highest ARS input concentration of 5.0 mM, the amounts of ARS sorbed were 78 and 93 mmol/kg, corresponding to a mass of 2.5% and 2.9% on Dol and HDol. Such small percentages will not typically show up in the FTIR spectra, which explains why none of the ARS absorption bands were observed in Figure 5.

3.6. SEM Observation and Particle Size Analyses

The SEM observation of Dol and HDol before ARS sorption can be seen in Figure 6. Essentially, there is not much change in crystal morphology, nor particle size before or after the heat treatment. For the particle size analyses of Dol, the surface weighted mean particle size is 14 μm while the volume weighted mean particle size is 66 μm and 63% of the particles had sizes of 2–63 μm . In contrast, the surface weighted mean particle size of HDol is 21 μm , while the volume weighted mean particle size is 67 μm and 55% of the particles had sizes of 2–63 μm . The results suggest a slight increase in particle size due to heating, which may be attributed to slight crystal growth during the heating process. But, overall, the difference between these two materials is small.

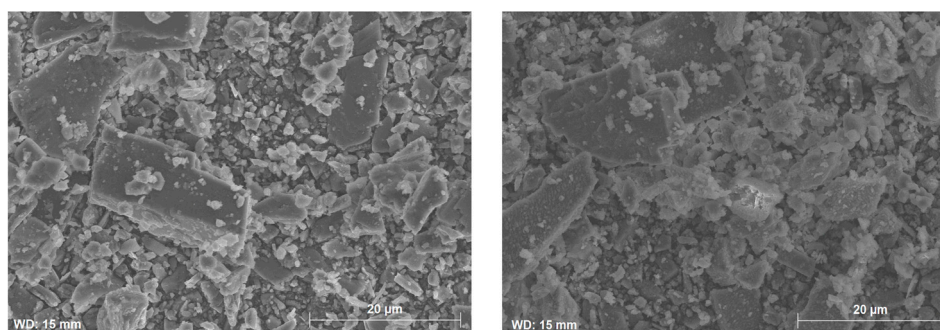


Figure 6. SEM images of Dol (left) and HDol (right), showing rough particle size distribution and crystal morphology.

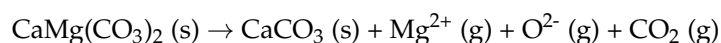
3.7. Discussion

Earlier studies showed that the sulfonic acid and/or its OH groups of ARS can react with calcium [35]. Depending on solution pH, three species of the oxidized forms of ARS would be present and electrochemical reduction may lead to dissociation of four phenolic hydroxyl groups as solution pH increases, which may result in formation of a total of 7 different species, with negative charges located on different O atoms [42]. Additionally, the binding between Ca^{2+} and ARS could be due to salt type, by which the Ca^{2+} forms complexes with O atoms attached to C1 and C2, or to chelate-type, by which the Ca^{2+} forms complexes with O atoms attached to C1 and C9 [19]. These types of binding could be illustrated in Figure 7. For the former case, the binding between Ca^{2+} with ARS could be 1:1, or 1:2 in a dimeric formation (Figure 7). On the Dol or HDol surfaces, the electrostatic and complexation interactions could result in different tilting angles, which could result in difference in ARS sorption capacities (Figure 7).

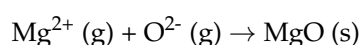
The bonding between ARS and Ca^{2+} was used for Ca stain [35], it is, thus, anticipated that calcite would be able to adsorb ARS. However, our preliminary studies using 0.1 and 0.2 mM ARS for its sorption on raw calcite and calcite heated to 600 and 800 °C resulted in similar sorption (about 70% removal). About 99% removal was achieved for HCal and aragonite heated to 1000 °C (data not published due to patent application). Dolomite has a typical formula of $\text{CaMg}(\text{CO}_3)_2$ and the presence of Ca^{2+} should also facilitate ARS sorption. It is likely that the presence of Mg^{2+} also forms complexation with ARS [19]. Accordingly, when ARS is sorbed on Dol or HDol surfaces, ARS could interact with Ca^{2+} or Mg^{2+} on Dol or HDol surfaces via the salt-type or chelate-type interactions.

In this study, with the assumed specific surface area (SSA) of 10 m^2/g and S_m value of 80 mmol/kg, the ARS sorption on Dol would form a relatively compact monolayer arrangement with a dipping angle about 40–50 degrees. In contrast, at the ARS sorption capacity of 138 mmol/kg on HDol, the ARS arrangement would be almost in a vertical monolayer arrangement using the same SSA value. By electrostatic interaction, the Ca^{2+} or Mg^{2+} will interact with the sulfonate group, which will result in a vertical or tilted ARS orientation on Dol or HDol surfaces (Figure 7).

In a more recent study [44], it was proposed that Dol decomposes in three stages, with the first stage occurring at 769 °C with the following reaction:



The second stage is the formation of MgO:



and the third stage is for the decomposition of calcite at 950 °C:



As the Dol was heated to 800 °C for 3 h, the chemical reaction during heating is: $\text{CaMg}(\text{CO}_3)_2 \rightarrow \text{CaCO}_3 + \text{MgO} + \text{CO}_2$. The differential thermal analyses (DTA) curve showed two endothermic peaks at 772 and 834 °C with the first peak due to the formation of MgO, CaCO₃, and CO₂, and the second peak represents Cal decomposition with formation of CaO and further CO₂ release [45]. Thus, the possibility of increased ARS sorption could be due to the slight increase in Ca²⁺ on surface coverage, which could facilitate more interactions between ARS and HDol via the salt type or chelate-type interactions. Also, the formation of MgO after heating may induce the formation of non-crystalline Mg(OH)₂ precipitates in aqueous suspension. Thus, further studies on interactions between Mg(OH)₂ and ARS are warranted.

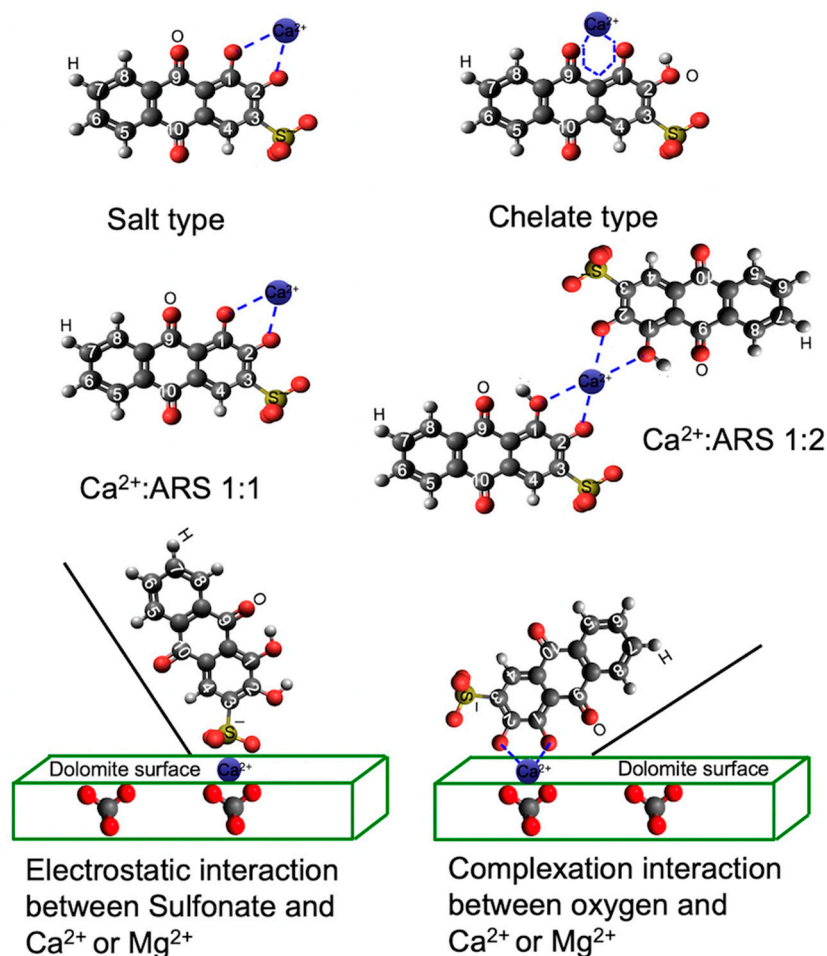


Figure 7. Illustration of interactions between ARS and Dol or HDol under electrostatic interaction or complexation interaction.

4. Conclusions

The removal of emerging contaminants by Earth materials was demonstrated in this study using alizarin red S (ARS) as a contaminant and dolomite before and after heat treatment as the sorbents under different physico-chemical conditions. The ARS removal capacity increased from 80 mmol/kg to 140 mmol/kg, about 75% in comparison to raw dolomite. The affinity increased by a factor of 4 after heat treatment. Significant increase in ARS removal was also found under kinetic, pH, ionic strength, and temperature conditions. XRD results suggested minute formation of calcite due to decomposition of dolomite after being heated at 800 °C for 4 h. No crystalline ARS was detected by XRD in the solid after being centrifuged and dried, indicating no ARS removal was via precipitation. As ARS may form complexation in addition to electrostatic interactions with Ca²⁺ on solid surface, the conversion from dolomite to calcite would remove some MgO from the surface and

increase the interactions between ARS and Ca^{2+} . Thus, the heat treatment of dolomite explored in this study shows a new perspective of using vast Earth materials such as calcite and dolomite in addition to clay minerals for the removal of emerging contaminants from water.

Author Contributions: Conceptualization, Z.L. and S.X.; methodology, Z.L.; investigation, A.R., A.B. and S.X.; resources, Z.L.; data curation, A.R. and A.B.; writing—original draft preparation, Z.L.; writing—review and editing, Z.L.; visualization, Z.L.; supervision, Z.L.; project administration, Z.L.; funding acquisition, Z.L. All authors have read and agreed to the published version of the manuscript.

Funding: This work was supported by a grant from WiSys, for the study of dye removal using carbonated minerals and another grant from WiSys for Scientist in Residency, and by a grant from Fresh Water Collaborative of Wisconsin to Engaging Undergraduate Students in Cutting-Edge Research on Use of Earth Materials for the Removal of Contaminants Including Dyes and Per- and Poly-fluorinated Substances.

Data Availability Statement: The data presented in this study are available on request from the corresponding author due to the privacy pertaining to patent application.

Acknowledgments: The authors from the University of Wisconsin – Parkside greatly appreciate the support from the Provost Office for provide URAP to the second and third authors, the Dean of the College of Natural and Health Science to encourage the first author to train undergraduates in cutting edge researches that lead to peer-reviewed publications, and Lori Allen for Chemistry Department to train the students for XRD and FTIR operations.

Conflicts of Interest: The authors declare no conflict of interests.

References

1. Modi, S.; Yadav, V.K.; Gacem, A.; Ali, I.H.; Dave, D.; Khan, S.H.; Yadav, K.K.; Rather, S.U.; Ahn, Y.; Son, C.T.; et al. Recent and emerging trends in remediation of methylene blue dye from wastewater by using zinc oxide nanoparticles. *Water* **2022**, *14*, 1749. [[CrossRef](#)]
2. Gupta, V.K. Application of low-cost adsorbents for dye removal—A review. *J. Environ. Manag.* **2009**, *90*, 2313–2342. [[CrossRef](#)]
3. Katheresan, V.; Kansedo, J.; Lau, S.Y. Efficiency of various recent wastewater dye removal methods: A review. *J. Environ. Chem. Eng.* **2018**, *6*, 4676–4697. [[CrossRef](#)]
4. Khan, M.D.; Singh, A.; Khan, M.Z.; Tabraiz, S.; Sheikh, J. Current perspectives, recent advancements, and efficiencies of various dye-containing wastewater treatment technologies. *J. Water Process Eng.* **2023**, *53*, 103579. [[CrossRef](#)]
5. Ganaie, R.J.; Rafiq, S.; Sharma, A. Recent advances in physico-chemical methods for removal of dye from wastewater. In Proceedings of the International Conference on Advance Earth Sciences & Foundation Engineering, Mohali, India, 23–24 June 2022; IOP Publishing: Bristol, UK, 2023; Volume 1110, p. 012040.
6. Ngulube, T.; Gumbo, J.R.; Masindi, V.; Maity, A. An update on synthetic dyes adsorption onto clay based minerals: A state-of-art review. *J. Environ. Manag.* **2017**, *191*, 35–57. [[CrossRef](#)] [[PubMed](#)]
7. Amari, A.; Gannouni, H.; Khan, M.I.; Almesfer, M.K.; Elkhaleefa, A.M.; Gannouni, A. Effect of structure and chemical activation on the adsorption properties of green clay minerals for the removal of cationic dye. *Appl. Sci.* **2018**, *8*, 2302. [[CrossRef](#)]
8. Li, Z.; Potter, N.; Rasmussen, J.; Weng, J.; Lv, G. Removal of rhodamine 6G with different types of clay minerals. *Chemosphere* **2018**, *202*, 127–135. [[CrossRef](#)] [[PubMed](#)]
9. Rao, W.; Piliouras, P.; Wang, W.; Guido, A.; Kugler, K.; Sieren, B.; Wang, L.; Lv, G.; Li, Z. Zwitterionic dye rhodamine B (RhB) uptake on different types of clay minerals. *Appl. Clay Sci.* **2020**, *197*, 105790. [[CrossRef](#)]
10. Boucif, F.; Marouf-Khelifa, K.; Batonneau-Gener, I.; Schott, J.; Khelifa, A. Preparation, characterisation of thermally treated Algerian dolomite powders and application to azo-dye adsorption. *Powder Technol.* **2010**, *201*, 277–282. [[CrossRef](#)]
11. Boucif, F.; Merouani, D.R.; Marouf-Khelifa, K.; Khelifa, A. Adsorption of Orange I by modified dolomite: Performance and mechanism. *Int. J. Environ. Sci. Technol.* **2021**, *18*, 3179–3188. [[CrossRef](#)]
12. Medjdoubi, A.; Hachemaoui, M.; Boukoussa, B.; Hakiki, A.; Bengueddach, A.; Hamacha, R. Adsorption behavior of Janus Green B dye on Algerian diatomite. *Mater. Res. Express* **2019**, *6*, 085544. [[CrossRef](#)]
13. Abdullah, S.F.A.; Saleh, S.S.M.; Mohammad, N.F.; Idris, M.S.; Saliu, H.R. Effect of thermal treatment on natural dolomite. In Proceedings of the 1st International Conference on Green Materials ICoGMPAC 2021, Perlis, Malaysia, 12 October 2021; IOP Publishing: Bristol, UK; Volume 2080, p. 012009.
14. Zahuri, A.A.; Abdul Patah, M.F.; Kamarulzaman, Y.; Hashim, N.H.; Thirumoorthi, T.; Wan Mohtar, W.H.M.; Mohd Hanafiah, Z.; Amir, Z.; Wan-Mohtar, W.A.A.Q.I. Decolourisation of real industrial and synthetic textile dye wastewater using activated dolomite. *Water* **2023**, *15*, 1172. [[CrossRef](#)]

15. Shirazi, E.K.; Metzger, J.W.; Fischer, K.; Hassani, A.H. Simultaneous removal of a cationic and an anionic textile dye from water by a mixed sorbent of vermicompost and Persian charred dolomite. *Chemosphere* **2019**, *234*, 618–629. [[CrossRef](#)]
16. Ziane, S.; Marouf-Khelifa, K.; Benmekki, H.; Schott, J.; Khelifa, A. Removal of a reactive textile azo dye by dolomitic solids: Kinetic, equilibrium, thermodynamic, and FTIR studies. *Desal. Water Treat.* **2015**, *56*, 695–708. [[CrossRef](#)]
17. Amen, R.; Elsayed, I.; Hassan, A.-B. Sustainable and economical dolomite-modified biochar for efficient removal of anionic dyes. *Arab. J. Chem.* **2023**, *16*, 105125. [[CrossRef](#)]
18. Elshimy, A.S.; Abdel-Gawwad, H.A.; Al-Dossari, M.; Abd EL-Gawaad, N.S.; Bonilla-Petriciolet, A.; Badawi, M.; Mobarak, M.; Lima, E.C.; Selim, A.Q.; Seliem, M.K. Utilization of alkali-activated dolomite waste toward the fabrication of an effective adsorbent: Experimental study and statistical physics formalism for the removal of methylene blue and crystal violet. *J. Phys. Chem. Solids* **2023**, *180*, 111442. [[CrossRef](#)]
19. Lemlikchi, W.; Sharrock, P.; Fiallo, M.; Nzihou, A.; Mecherri, M.O. Hydroxyapatite and Alizarin sulfonate ARS modeling interactions for textile dyes removal from wastewaters. *Procedia Eng.* **2014**, *83*, 378–385. [[CrossRef](#)]
20. Gregory, C.A.; Gunn, W.G.; Peister, A.; Prockop, D.J. An Alizarin red-based assay of mineralization by adherent cells in culture: Comparison with cetylpyridinium chloride extraction. *Anal. Biochem.* **2004**, *329*, 77–84. [[CrossRef](#)]
21. Rheima, A.M.; Mahmood, R.S.; Hussain, D.H.; Abbas, Z.S. Study the adsorption ability of alizarin red dye from their aqueous solution on synthesized carbon nanotubes. *Dig. J. Nanomater. Biostructures* **2021**, *16*, 11–18. [[CrossRef](#)]
22. Al-Salihi, K.J.; Alfatlawi, W.R. Synthesis and characterization of low-cost adsorbent and used for Alizarin yellow GG and alizarin Red S dyes removal from aqueous solutions. In Proceedings of the 1st International Conference on Sustainable Engineering and Technology (INTCSET 2020), Baghdad, Iraq, 15–16 December 2020; IOP Publishing: Bristol, UK, 2021; Volume 1094, p. 012175.
23. Rehman, R.; Mahmud, T.; Anwar, J.; Salman, M.; Shafique, U.; Zaman, W.U.; Ali, F. Removal of alizarin red s (dye) from aqueous media by using alumina as an adsorbent. *J. Chem. Soc. Pak.* **2011**, *33*, 228–232.
24. Friedman, G.M. Identification of carbonate minerals by staining methods. *J. Sediment. Res.* **1959**, *29*, 87–97.
25. Dickson, J.A.D. Carbonate identification and genesis as revealed by staining. *J. Sediment. Res.* **1966**, *36*, 491–505.
26. Fu, E.; Somasundaran, P. Alizarin Red S as a flotation modifying agent in calcite-apatite systems. *Int. J. Miner. Process.* **1986**, *18*, 287–296. [[CrossRef](#)]
27. Adeogun, A.I.; Babu, R.B. One-step synthesized calcium phosphate-based material for the removal of alizarin S dye from aqueous solutions: Isothermal, kinetics, and thermodynamics studies. *Appl. Nanosci.* **2021**, *11*, 1–13. [[CrossRef](#)]
28. Wu, L.; Forsling, W.; Holmgren, A. Surface complexation of calcium minerals in aqueous solution: 4. The Complexation of Alizarin Red S at Fluorite–Water Interfaces. *J. Colloid Interface Sci.* **2020**, *224*, 211–218. [[CrossRef](#)] [[PubMed](#)]
29. Shirazi, E.K.; Metzger, J.W.; Fischer, K.; Hassani, A.H. Removal of textile dyes from single and binary component systems by Persian bentonite and a mixed adsorbent of bentonite/charred dolomite. *Colloids Surf. A* **2020**, *598*, 124807. [[CrossRef](#)]
30. Kurtulbaş, E.; Yıldırım, E.; Emik, S.; Şahin, S. A detailed study on the sorption characteristics of humic acid onto calcined dolomite. *J. Mol. Struct.* **2020**, *1219*, 128606. [[CrossRef](#)]
31. Storti, F.; Balsamo, F. Particle size distributions by laser diffraction: Sensitivity of granular matter strength to analytical operating procedures. *Solid Earth* **2010**, *1*, 25–48. [[CrossRef](#)]
32. Al-Ghouti, M.A.; Da'ana, D.A. Guidelines for the use and interpretation of adsorption isotherm models: A review. *J. Hazard. Mater.* **2020**, *393*, 122383. [[CrossRef](#)]
33. Rehman, R.; Abbas, A.; Murtaza, S.; Anwar, J.; Mahmud, T.; Akbar, S. Adsorption parameters optimization for removal of alizarin red-S and brilliant blue FCF dyes from water using *Abelmoschus esculentus* stem powder. *J. Chem. Soc. Pak.* **2013**, *35*, 443–448.
34. Shi, Y.; Baker, J.; Feng, C.; Wang, X.; Li, Z. Removal of toluidine blue from water using 1: 1 layered clay minerals. *Adv. Powder Technol.* **2022**, *33*, 103608. [[CrossRef](#)]
35. Puchtler, H.; Meloan, S.N.; Terry, M.S. On the history and mechanism of alizarin and alizarin red S stains for calcium. *J. Histochem. Cytochem.* **1969**, *17*, 110–124. [[CrossRef](#)]
36. Gautam, R.K.; Banerjee, S.; Gautam, P.K.; Rawat, V.; Kumar, A.; Singh, S.K.; Chattopadhyaya, M.C. Biosorption of an acidic dye, alizarin red S onto biosorbent of mustard husk: Kinetic, equilibrium modeling and spectroscopic analysis. *Asian J. Res. Chem.* **2014**, *7*, 417–425.
37. El-Nahass, M.M.; Zeyada, H.M.; El-Ghamaz, N.A.; Awed, A.S. Structural investigation, thermal analysis and AC conduction mechanism of thermally evaporated alizarin red S thin films. *Optik* **2018**, *170*, 304–313. [[CrossRef](#)]
38. Balakrishnan, G.; Velavan, R.; Batoo, K.M.; Raslan, E.H. Microstructure, optical and photocatalytic properties of MgO nanoparticles. *Results Phys.* **2020**, *16*, 103013. [[CrossRef](#)]
39. Blanton, T.N.; Barnes, C.L. Quantitative analysis of calcium oxide desiccant conversion to calcium hydroxide using X-ray diffraction. *Adv. X-ray Anal.* **2005**, *28*, 45–51. [[CrossRef](#)]
40. Maor, Y.; Toffolo, M.B.; Feldman, Y.; Vardi, J.; Khalaily, H.; Asscher, Y. Dolomite in archaeological plaster: An FTIR study of the plaster floors at Neolithic Motza. *Isr. J. Archaeolog. Sci. Rep.* **2023**, *48*, 103862. [[CrossRef](#)]
41. Ji, J.; Ge, Y.; Balsam, W.; Damuth, J.E.; Chen, J. Rapid identification of dolomite using a Fourier Transform Infrared Spectrophotometer (FTIR): A fast method for identifying Heinrich events in IODP Site U1308. *Mar. Geol.* **2009**, *258*, 60–68. [[CrossRef](#)]
42. Turcanu, A.; Bechtold, T. pH Dependent redox behaviour of Alizarin Red S (1, 2-dihydroxy-9, 10-anthraquinone-3-sulfonate)–Cyclic voltammetry in presence of dispersed vat dye. *Dye. Pigment.* **2011**, *91*, 324–331. [[CrossRef](#)]

43. Chin, Y.P.; Raof, S.F.A.; Sinniah, S.; Lee, V.S.; Mohamad, S.; Manan, N.S.A. Inclusion complex of Alizarin Red S with β -cyclodextrin: Synthesis, spectral, electrochemical and computational studies. *J. Molec. Struct.* **2015**, *1083*, 236–244. [[CrossRef](#)]
44. Resio, L.C. Dolomite thermal behaviour: A proposal to establish a definitive decomposition mechanism in a convective air atmosphere. *Open Ceram.* **2023**, *15*, 100405. [[CrossRef](#)]
45. Shahraki, B.K.; Mehrabi, B.; Dabiri, R. Thermal behavior of Zefreh dolomite mine (Central Iran). *J. Min. Metall. B Metall.* **2009**, *45*, 35–44. [[CrossRef](#)]

Disclaimer/Publisher's Note: The statements, opinions and data contained in all publications are solely those of the individual author(s) and contributor(s) and not of MDPI and/or the editor(s). MDPI and/or the editor(s) disclaim responsibility for any injury to people or property resulting from any ideas, methods, instructions or products referred to in the content.